Contents list available at IJRED website

International Journal of Renewable Energy Development

Journal homepage: https://ijred.undip.ac.id

Research Article

Numerical assessment of meshless method for studying nanofluid natural convection in a corrugated wall square cavity

Youssef Es-Sabry[a], Mohammed Jeyar[b], Elmiloud Chaabelasri[a]*, Dris Bahia[c]

[a]*LPTPME Laboratory, Faculty of Sciences, Mohammed 1St University, Oujda, 60000, Morocco*

[b]*Higher School of Technologie of Oujda, Mohammed 1St University, Oujda, 60000, Morocco*

[c]*Multidisciplinary Faculty of Nador, Mohammed 1St University, Nador, Morocco*

Abstract. This study aims to investigate the impact of various factors, such as wall shape, Rayleigh number, and volume fraction of nanoparticles, on natural convection in a square cavity that is filled with a mixture of Al2O3 solid particles and liquid water. The research employs numerical simulations based on the radial basis function meshless method and the artificial compressibility technique. The results of the study showed that the temperature distribution in the cavity was mostly uniform, except in the vicinity of the hot wall, while the flow was primarily dominated by convection as the Rayleigh number increased. Furthermore, the heat transfer rate increased with the volume fraction of nanoparticles, indicating the significance of nanoparticles in improving the thermal performance of the system. Additionally, the study found that the average Nusselt number, which characterizes the heat transfer efficiency, was highest when the cavity had a wavy wall. For single and double wavy walls, there were respective enhancements of 32% and 6% compared to a regular wall. Additionally, the Nusselt number increased as the volume fraction of nanoparticles, indicating a significant influence of nanoparticle concentration and wall geometry on the fluid flow and heat transfer characteristics in the square cavity. Consequently, this study's outcomes provide crucial insights into designing and optimizing thermal management systems, particularly those utilizing nanofluids.

Keywords: Natural convection, Nanofluid, Square cavity, Corrugated wall, Meshless method, Radial basis function

Received: 27th March 2023; Revised: 2nd July 2023; Accepted: 27th July 2023; Available online: 2nd August 2023

1. Introduction

The improvement of heat transfer in heat exchangers has long been of interest to industrialists and, by extension, to scientific researchers. Demand for cavities, which are commonly used to cool electronic components, is on the rise. The heat transfer inside these cavities can be significantly improved by various methods, including the use of nanofluids with high thermal conductivity instead of conventional fluids like air or water (Keshtkar *et al* 2018; Aghakhani *et al.* 2018 ; Shahsavar *et al.* 2021 ; Miroshnichenko *et al.*2018 ; Muhammad *et al.* 2020 ; Kadhim *et al.* (2022) and Shoeibi *et al* (2023)). Additionally, designing alternative cavity configurations with or without obstacles can change flow behavior and increase heat transfer. Researchers have used different methods to study the impact of nanofluids on heat transfer in different types of cavities.

Due to extensive research in the field, some authors have focused on reviewing existing studies. Recent studies have explored natural convection flow and heat transfer in enclosures of various shapes. Rahimi *et al.* (2019) conducted a review of the latest work in this area, analyzing the effects of different physical and thermal boundary conditions, governing parameters, and fluid parameters on convective flow and heat transfer performance in square and rectangular, trapezoidal, triangular, and parallelogram-shaped enclosures. Similarly, Das *et al.* (2017) summarized work on flow in triangular, trapezoidal, parallelogram-shaped enclosures, and nanofluid-filled enclosures. Bairi *et al.*(2014)provided an overview of natural convection in parallelogram-shaped cavities, relevant for technical applications.

The improvement of thermal performance in rectangular cavities is still a focus of research. Alqaed *et al.* (2022) recently numerically studied natural convection of an alumina/H2O nanofluid in a cavity with two hot triangular blades on the bottom wall, insulated side walls, and a low-temperature top wall. They analyzed heat transfer by estimating variations of Nusselt number, Bejan number, and entropy generation rate with cavity angle, Hartmann number, and Rayleigh number. The study showed that as the Bejan number decreased, the Nusselt number and entropy generation rate increased with the Rayleigh number but not with increasing Hartmann numbers. The maximum values of entropy generation and Nusselt number and the minimum value of Bejan were found at a 30° angle. The modification of geometry and use of a high thermal conductivity fluid significantly improved thermal performance.

Zarei *et al.*(2022) used a finite volume method with the SIMPLE algorithm to study two-dimensional natural convection in a corrugated wall cavity filled with a water-based nanofluid. They analyzed the effect of wall wavelength, amplitude, and volume fraction of nanoparticles on heat transfer for a Rayleigh number of 104. Results showed that the volume fraction had the greatest effect on heat transfer and increased the average

*Corresponding author
Email: chaabelasri@gmail.com (E. Chaalbelasri)

https://doi.org/10.14710/ijred.2023.53277
ISSN: 2252-4940/© 2023.The Author(s). Published by CBIORE

Nusselt number by 2.5 times when increasing from 0 to 0.04. The wall wavelength had the least effect on heat transfer.

Hu *et al.* (2022) in their study extended the scope of nanofluids research by using the finite volume method to examine the oscillatory characteristics of natural convection near its maximum density in a narrow horizontal ring. The equations used were written in polar coordinates. They analyzed the effect of variables such as the nanoparticle volume fraction, Rayleigh number, and density inversion parameter on the flow pattern and heat transfer capacity. A significant finding of the study is that the addition of nanoparticles stabilizes and preserves the symmetry of the flow structure, and the heat transfer by natural convection is improved with an increase in the nanoparticle fraction.

The advent of meshless methods has expanded the spectrum of numerical methods available, offering high flexibility in handling complex geometries(Sophy *et al.* 2002 ; Zhang *et al.* 2015 ; Jeyar *et al.* 2022 ; Luo *et al.* 2015 ; Najafi *etal.* 2014 ; Pranowo *et al.* 2021 ; Sheikhi *et al* 2018). In this vein, the work of Nuwairan*et al.* (2023) analyzed natural heat convection in square and equilateral triangular cavities using a collocation-based meshless method using local radial basis functions (RBF). The nanofluids studied were Cu-water or water-nanoparticle mixtures with a volume fraction range of 0.2. The RBF method was used to approximate the partial derivatives in the governing equations. Results showed that the addition of nanoparticles significantly improved heat transfer compared to pure fluid. As the Rayleigh number increased, heat transfer dominated conduction, resulting in heat transfer from the hot walls to the cool walls.

Pekmen and Oztop (2022) investigated the effect of a periodic magnetic field on the natural convection of a nanofluid in an isosceles triangular cavity using a meshless method based on radial basis function-based unit partition method. The numerical solution of the dimensionless time-independent equations was carried out. The results analyze the effect of partially or fully tilted magnetic fields, as well as the Hartmann parameter and period variation. It was concluded that an increase in the Hartmann number suppresses fluid flow and heat transfer, with a full magnetic field having a greater suppressing effect than a partial magnetic field. In a triangle configuration with a horizontal periodic magnetic field, the suppression by a full magnetic field was greater than that by a partial magnetic field.

The literature review above indicates that the issue of natural convection in a rectangular container remains unresolved, particularly when new mixed fluids are used in such a cavity. This paper aims to conduct a more extensive investigation into the topic of natural convection of nanofluid in square containers with varying wall shapes and under varying conditions of heat transfer and nanoparticle volume fraction.

The structure of this paper is as follows. In Section 2, we provide an overview of the governing equations used to model the natural convection of nanofluids. In Section 3, the meshless method is presented as well as the artificial compressibility technique. In Section 4, we present numerical results and discussions. Section 5 is devoted to closing remarks.

2. Problems definition and governing equations

2.1 Problem definition

In this research, a numerical analysis of heat transfer and fluid flow within a cavity with three distinct walls is conducted. The cavity and the analyzed walls are shown in Figure 1. The three walls are aligned vertically and have the following shapes: a wavy wall (w_1), a zig-zag wall (w_2), and a square wall (w_3). The

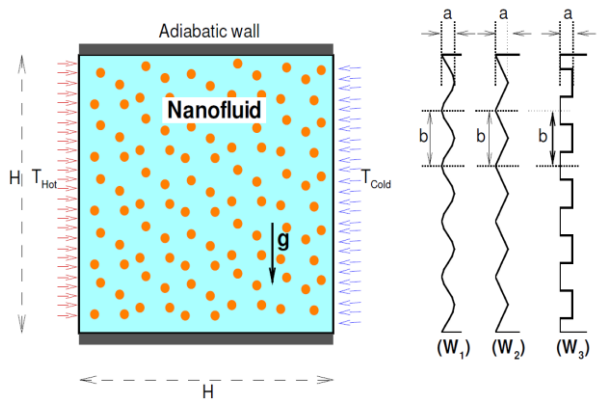

Fig 1. Geometry of physical problem

amplitude of the waves in the wavy wall, or the height of the zig-zag or square shapes in the wall, is represented by distance a, which is set to 0.05. The distance b is set to 0.2 so that there are N=5 waves, zig-zags, or squares on each wall. The two vertical walls are kept at constant and uniform temperatures, T_h and T_c, respectively, and the horizontal walls are considered adiabatic. The cavity is filled with a Newtonian, incompressible, and laminar Al_2O_3-water nanofluid. The thermophysical properties of the nanofluid are assumed to be constant, except for the density change, which is modeled using the Boussinesq approximation in the buoyancy term (Bejan, 2013). The water and Al_2O_3 phases are considered to be in thermal equilibrium, with no temperature or velocity difference between them, and are modeled as a single-phase homogeneous fluid. The effects of thermal radiation and viscous dissipation are not taken into account, and the gravitational acceleration is only considered in the y-direction.

2.2 Governing Equations

Considering the above assumptions, the continuity, momentum, and energy equations governing the steady-state heat transfer and laminar flow of the nanofluid are as follows (Mahmoodi &Sebdani,2012):

$$\begin{cases} u_x + v_y = 0 \\ u_t + (uu_x + vu_y) = -\frac{1}{\rho_{nf}} p_x + (u_{xx} + u_{yy}) \\ v_t + (uv_x + vv_y) = -\frac{1}{\rho_{nf}} p_y + (v_{xx} + v_{yy}) + \frac{g(\rho\beta)_{nf}}{\rho_{nf}} (T - T_c) \\ T_t + (uT_x + vT_y) = \alpha_{nf} (T_{xx} + T_{yy}) \end{cases} \quad (1)$$

where u, and v are the components of the velocity vector in (x, y) directions, respectively. The indicatives x, y, xx, and yy denote the first and second differentiation operators with respect to x and y, T is the nanofluid temperature, ρ_{nf} is the nanofluid density, ν_{nf} is the nanofluid kinematic viscosity, g is the gravitational acceleration, β_{nf} is the nanofluid thermal expansion, and α_{nf} is the nanofluid thermal diffusivity.

Following dimensionless variables are used for converting the above equations in dimensionless form:

$$X = \frac{x}{L}, Y = \frac{y}{L}, t = \frac{\tilde{t}\alpha_f}{L^2}, u = \frac{L}{\alpha_f} U, v = \frac{L}{\alpha_f},$$
$$p = \frac{L^2}{\rho\alpha_f^2}, \theta = \frac{T - T_c}{T_h - T_c} \quad (2)$$

Using the above dimensionless variables, the system of governing equations takes the following dimensionless form:

$$\begin{cases} U_x + V_y = 0 \\ U_{\tilde{t}} + (UU_{\mathrm{x}} + VU_{\mathrm{y}}) = -\frac{\rho_f}{\rho_{nf}} P_x + \frac{\nu_{nf}}{\nu_f}(U_{\mathrm{xx}} + U_{\mathrm{yy}}) \\ V_{\tilde{t}} + (UV_{\mathrm{x}} + VV_{\mathrm{y}}) = -\frac{\rho_f}{\rho_{nf}} P_y + \frac{\nu_{nf}}{\nu_f}(V_{\mathrm{xx}} + V_{\mathrm{yy}}) + \frac{(\rho\beta)_{\mathrm{nf}}}{\rho_f \rho_{nf}} Ra \Pr \theta \\ \theta_{\tilde{t}} + (U\theta_{\mathrm{x}} + V\theta_{\mathrm{y}}) = \frac{\alpha_{nf}}{\alpha_f}(\theta_{\mathrm{xx}} + \theta_{\mathrm{yy}}) \end{cases} \quad (3)$$

where Pr and Ra represent the Prandtl and Rayleigh numbers, respectively, and are defined as follows:

$$\Pr = \frac{\nu_f}{\alpha_f}, \quad Ra = \frac{g\beta_f(\mathrm{T_h} - \mathrm{T_c})\mathrm{L}^3}{\nu_f \alpha_f} \quad (4)$$

Furthermore, Dirichlet and Newmann boundary conditions are used to update the flow field (U, V, θ) on the boundary walls of the cavity. With these two boundary approximations, the dimensionless boundary conditions are formulated as follows:

$\frac{\partial\theta}{\partial n}=0$ $\frac{\partial\theta}{\partial n} = 0$For Temperature,$\frac{\partial\theta}{\partial n} = 0$, on the upper and lower horizontal walls, $\theta(X = 0, Y) = \theta_h = 1$ on the left vertical wall and $\theta(X = L, Y) = \theta_c = 0$ on the right vertical wall. For Velocity, $u=v=0$ on all walls.

The local Nusselt number is one of the most commonly used numbers to measure the rate of heat transfer. It represents the ratio of convective to conductive heat transfer across a boundary and is given by

$$Nu_l = -\frac{K_{nf}}{K_f}\frac{\partial\theta}{\partial x}\Big|_{X=0} \quad (5)$$

The average Nusselt number is calculated by integrating the local Nusselt number along the hot wall of the cavity as follows:

$$Nu_{avg} = \int_0^L Nu_l dx \quad (6)$$

2.3 Nanofluid thermophysical properties

Thermophysical properties of water and Al_2O_3 nanoparticles are given in Table 1. The effective density of the nanofluid is calculated based on the density of the base fluid (ρ_f), the density of the solid nanoparticles (ρ_s), and the volume fraction of the particles (ϕ), as follows (Khanafer *et al*., 2003):

$$\rho_{\mathrm{nf}} = (1 - \phi)\rho_f + \phi\rho_s \quad (7)$$

The thermal capacity of the nanofluid is determined as:

$$(\rho c_p)_{\mathrm{nf}} = (1 - \phi)(\rho c_p)_f + \phi(\rho c_p)_s \quad (8)$$

Table 1
Thermophysical properties of water and nanoparticles.

Properties	H_2O	Al_2O_3
ρ[Kg/m^3]	997.1	3970
c_p[J/Kg/K]	4179	765
k[W/m/K]	0.613	40
β[1/K]×10^{-5}	1.67	0.85
μ[Kg/m/s]	0.001	-

where $(\rho c_p)_f$ is the thermal capacity of the base fluid, and $(\rho c_p)_s$ is the thermal capacity of the solid particles. Thermal diffusivity of the nanofluid is determined by

$$\alpha_{\mathrm{nf}} = \frac{k_{\mathrm{nf}}}{(\rho c_p)_{\mathrm{nf}}} \quad (9)$$

and the thermal expansion coefficient of the nanofluids can be determined as:

$$(\rho\beta)_{\mathrm{nf}} = (1 - \phi)(\rho\beta)_f + \phi(\rho\beta)_s \quad (10)$$

where $(\rho\beta)_{\mathrm{f}}$ and $(\rho\beta)_s$ are the thermal expansion coefficient of the base fluid and the solid particles, respectively. According to the Brinkman model (Brinkman 1952), the effective viscosity of the nanofluid is given by

$$\mu_{\mathrm{nf}} = \frac{\mu_{\mathrm{f}}}{(1-\phi)^{2.5}} \quad (11)$$

here μ_{f} represents the effective viscosity of the base fluid.

The effective thermal conductivity of the nanofluid is approximated using the Maxwell model (Maxwell 1904). This model allows us to express the effective thermal conductivity of the nanofluid as:

$$k_{\mathrm{nf}} = k_{\mathrm{f}}\left(\frac{k_{\mathrm{p}} + 2k_{\mathrm{f}} - 2\phi(k_{\mathrm{f}} - k_{\mathrm{p}})}{k_{\mathrm{p}} + 2k_{\mathrm{f}} + 2\phi(k_{\mathrm{f}} - k_{\mathrm{p}})}\right) \quad (12)$$

where k_{p} is the thermal conductivity of the base fluid, and k_{s} the thermal conductivity of solid particles. These relations have been widely used in the literature for numerical simulation of free convection of nanofluid (Aminossadati *et al.* (2009); Saleh *et al.* (2011); Sheikholeslami *et al.* (2016); Sheikhzadeh *et al.*(2011).

3. Description of the numerical method

When attempting to find a numerical solution for the equations (3), there are several challenges. The momentum equations contain a pressure gradient, and they cannot be solved without specifying the pressure term. In this work, we adopt the method of artificial compressibility proposed by Chorin (1997) to handle the pressure-velocity coupling. This method couples pressure with velocity by adding a pseudo-temporal derivative to the continuity equation, as follows:

$$P_{\tilde{t}} + \gamma(\mathrm{U_X} + U_Y) = 0 \quad (13)$$

Here, γ is an artificial compressibility parameter, a crucial but adjustable parameter that influences the convergence of the solution. In this study, a value of 10^{-5} was used to achieve convergence. For simplicity, the right-hand side elements of the above mathematical model (3) are rewritten in a compact form as follows:

$$\mathrm{L}(\boldsymbol{W}) = \begin{bmatrix} -\gamma(U_x + V_y) \\ -(UU_{\mathrm{x}} + VU_{\mathrm{y}}) - \frac{\rho_f}{\rho_{nf}} P_x + \frac{\nu_{nf}}{\nu_f}(U_{\mathrm{xx}} + U_{\mathrm{yy}}) \\ -(UV_{\mathrm{x}} + VV_{\mathrm{y}}) - \frac{\rho_f}{\rho_{nf}} P_y + \frac{\nu_{nf}}{\nu_f}(V_{\mathrm{xx}} + V_{\mathrm{yy}}) + \frac{(\rho\beta)_{\mathrm{nf}}}{\rho_f \rho_{nf}} Ra \Pr \theta \\ -(U\theta_{\mathrm{x}} + V\theta_{\mathrm{y}}) + \frac{\alpha_{nf}}{\alpha_f}(\theta_{\mathrm{xx}} + \theta_{\mathrm{yy}}) \end{bmatrix} \quad (14)$$

where $W = (P, U, V, \theta)^T$ is the unknown physical vector.

3.1 Spatial derivative Approximation

This work addresses the problem of interpolating an unknown function $W:\mathbb{R}^2 \to \mathbb{R}$ from N functional values $\{W(x_1),\ldots,W(x_N)\}$, where the centers $x_1,\ldots,x_N \in \Omega$ and $\Omega \subset \mathbb{R}^2$ is bounded domain and the centers are taken anywhere in the domain Ω. In local RBF approximation techniques, at every center $x_j \in \Omega$, the local interpolant (Kansa 1990):

$$W(x_j,t) = \sum_{x_k \in \Omega_j} \lambda_k(t)\phi\left(\left\|x_j - x_k\right\|,\varepsilon\right) \tag{15}$$

where $\lambda^j = (\lambda_1,\ldots,\lambda_n)$ is expansion coefficients and $\|x_j - x_k\|$ is the Euclidean distance between x_j and x_k. Here, $\phi\left(\left\|x_j - x_k\right\|,\varepsilon\right) = \sqrt{1-\varepsilon\|x_j - x_k\|^2}$ is a multiquadric function where ε is a shape parameter that plays a substantial role in the resulting accuracy (Bayona *et al.* (2011); Fasshauer *et al.* (2007); Liu *et al.* (2018); Uddin *et al.* (2014). Generally, the determination of the range of shape value can be obtained by using numerical tests. In this study, we use the formula employed in the work of Nuwairan *et al.* (2023).

$\Omega_j \subset \Omega$ is the local support domain for each node x_j and have n nearest centres with centre. The N number of $N \times N$ linear systems is

$$W^j = \phi^j \Gamma^j j = 1,\ldots,N \tag{16}$$

where Φ^j is the local matrix RBF, which elements are $\Phi_k^j = \Phi(\|x_k - x_j\|)$, where x_k and $x_j \in \Omega$. Applying the differential operator L to Equation (Sarra 2012)

$$\mathrm{L}(W(x_j,t)) = \sum_{x_k \in \Omega_j} \lambda_k(t)\mathrm{L}(\phi\left(\left\|x_j - x_k\right\|\right)) \tag{17}$$

The expression in (17) can be written as element-wise product of two vectors,

$$\mathrm{L}W^j = \Phi_{\mathrm{L}}^j \Gamma^j \tag{18}$$

where Γ^j is the $n \times 1$ vector of unknown coefficients, and ϕ_L^j is $1 \times n$ vector with entries $\mathrm{L}\phi(\|x_j - x_k\|)$. To eliminate the unknown coefficients, we rewrite Equation (16) as:

$$\Gamma^j = \left(\phi^j\right)^{-1} W^j, j = 1,\ldots,N \tag{19}$$

on substituting the values of Γ^j from (19) in (18) we have,

$$\mathrm{L}\boldsymbol{W}^j = \Phi_{\mathrm{L}}^j (\Phi^j)^{-1}\boldsymbol{W}^j = \mathrm{M}_{\mathrm{L}}^j \boldsymbol{W}^j \tag{20}$$

where,

$$\mathrm{M}_{\mathrm{L}}^j = \Phi_{\mathrm{L}}^j (\Phi^j)^{-1} \tag{21}$$

gives weight to centre x_j. For all centers, it gives

$$\mathrm{L}\boldsymbol{W} = \mathrm{M}_{\mathrm{L}}^j \boldsymbol{W} \tag{22}$$

where $\mathcal{M}_{\mathcal{L}}$ is $M \times M$ sparse differentiation matrix, each row has an $M - m$ zeros elements, where m is the stencil size in each local domain Ω_j. This differentiation matrix will be used to approximate the derivatives of the governing equations. Thus, the first and second derivatives are evaluated using the matrix $\mathcal{M}_x$, $\mathcal{M}_{xx}$, $\mathcal{M}_y$ and $\mathcal{M}_{yy}$ for the derivatives with respect to the x and y successively.

Accordingly, using the differentiation matrix, the right-hand side of the partial differential problem (3) can be approximated as:

$$\mathrm{L}(\boldsymbol{W}) = \begin{bmatrix} -\gamma(U_x + V_y) \\ -(U\mathrm{M}_x U + V\mathrm{M}_y U) - \frac{\rho_f}{\rho_{nf}}\mathrm{M}_x P + \frac{\nu_{nf}}{\nu_f}(\mathrm{M}_{xx}U + \mathrm{M}_{yy}U) \\ -(U\mathrm{M}_x V + V\mathrm{M}_y V) - \frac{\rho_f}{\rho_{nf}}\mathrm{M}_y P + \frac{\nu_{nf}}{\nu_f}(\mathrm{M}_{xx}V + \mathrm{M}_{yy}V) + \frac{(\rho\beta)_{nf}}{\rho_f \rho_{nf}} Ra\,\mathrm{Pr}\,\theta \\ -(U\mathrm{M}_x \theta + V\mathrm{M}_y \theta) + \frac{\alpha_{nf}}{\alpha_f}(\mathrm{M}_{xx}\theta + \mathrm{M}_{yy}\theta) \end{bmatrix} \tag{23}$$

3.2 Temporal approximation

After spatial local RBF approximation, we obtained the following system of ODEs

$$W_{\tilde{t}} = F(W) \tag{24}$$

in which $F(\mathrm{W}) = \mathcal{L}(\mathrm{W})$. For an ordinary differential equation computation, the fourth-order Runge-Kutta method has been taken (Chaabelasri 2019). These recursive steps are expressed as follows:

$$\begin{aligned} \tilde{\boldsymbol{W}}_1 &= F(\boldsymbol{W}^n) \\ \tilde{\boldsymbol{W}}_2 &= F(\boldsymbol{W}^n + \frac{\Delta t}{2}\tilde{\boldsymbol{W}}_1) \\ \tilde{\boldsymbol{W}}_3 &= F(\boldsymbol{W}^n + \frac{\Delta t}{2}\tilde{\boldsymbol{W}}_2) \\ \tilde{\boldsymbol{W}}_4 &= F(\boldsymbol{W}^n + \frac{\Delta t}{2}\tilde{\boldsymbol{W}}_3) \\ \boldsymbol{W}^{n+1} &= \boldsymbol{W}^n + \frac{\Delta t}{6}(\tilde{\boldsymbol{W}}_1 + 2\tilde{\boldsymbol{W}}_2 + 2\tilde{\boldsymbol{W}}_3 + \tilde{\boldsymbol{W}}_4) \end{aligned} \tag{25}$$

The purpose of our study is to examine the steady state solution, despite the fact that the governing equations are time dependent. Thus, the steady state is reached when the variations of the variables approach zero with the help of this method. The convergence criterion for the steady state is:

$$\|\theta^{n+1} - \theta^n\|_\infty \le \varepsilon_{err} \text{ and} \|U^{n+1} - U^n\|_\infty \le \varepsilon_{err} \tag{26}$$

Here n and $n+1$ denote two adjacent time steps and ε_{err} is taken equal to 10^{-5} in all cases.

4. Result and discussion

4.1 Grid independence and validation

A grid sensitivity analysis was performed to investigate steady-state natural convection and fluid flow in a square cavity filled with Al_2O_3-water nanofluid. The walls of the cavity are plane surfaces and the average Nusselt number along the heated wall was used to determine the number of nodes for numerical investigations. The grid independence solution was obtained using different numbers of nodes, including 1000, 2000, 3000, and 4000 nodes. The results for $\mathrm{Ra} = 10^5$ and $\phi = 0.1$ are shown in Table 2 and indicate that the solution becomes independent of the node number from 3000. Therefore, the uniform grid of 3000 nodes was selected due to its better balance between computational time and accuracy. The validity and accuracy of the numerical method were verified by comparing the average Nusselt number on the hot wall of the square cavity at $\phi = 0.1$ and various Rayleigh numbers with

Table 2
Comparison of average Nusselt numbers for different numbers of nodes at Ra = 10^4 and ϕ = 0.1

Number of nodes	Average Nusselt number
1000	2.3034
2000	2.7323
3000	2.7376
4000	2.7379

Table 3
Comparison of the average Nusselt numbers with those obtained by Basak *et al.* (2012) at ϕ = 0.1 and different Rayleigh numbers.

Parameter	Average Nusselt number	
Ra	**Present study**	**Basak** *et al.*
1000	1.3446	1.3901
10000	2.7376	2.4752
100000	5.0012	5.3050

those obtained by Basak *et al.* (2012). The results in Table 3 demonstrate that the code accurately reproduces the results reported inBasak *et al*. (2012).

4.2 Natural convection in a square cavity with one irregular lateral wall

In the initial part of this study, natural convection in a square cavity with one irregular lateral wall is analyzed. The irregular wall, which is located on the left side of the cavity, takes on three distinct shapes: corrugated wavy, zig-zag and square wall. The other walls of the cavity are flat. The cavity is filled with a mixture of Al_2O_3 solid particles and liquid water, with a Prandtl number of Pr= 6.2. The thermophysical properties of the solid particles Al_2O_3 and liquid water are outlined in Table 1. Numerical simulations are performed to examine the influence of the corrugated walls, Rayleigh number, and volume fraction of nanoparticles on the dimensionless temperature, stream function, and local and average Nusselt numbers.

In Figure 2, the isothermal lines are displayed for different values of the Rayleigh number and volume fraction of nanoparticles. For all three configurations, the overall characteristics of the isotherms remain unchanged, except for the region surrounding the left hot wall. The isotherms reflect

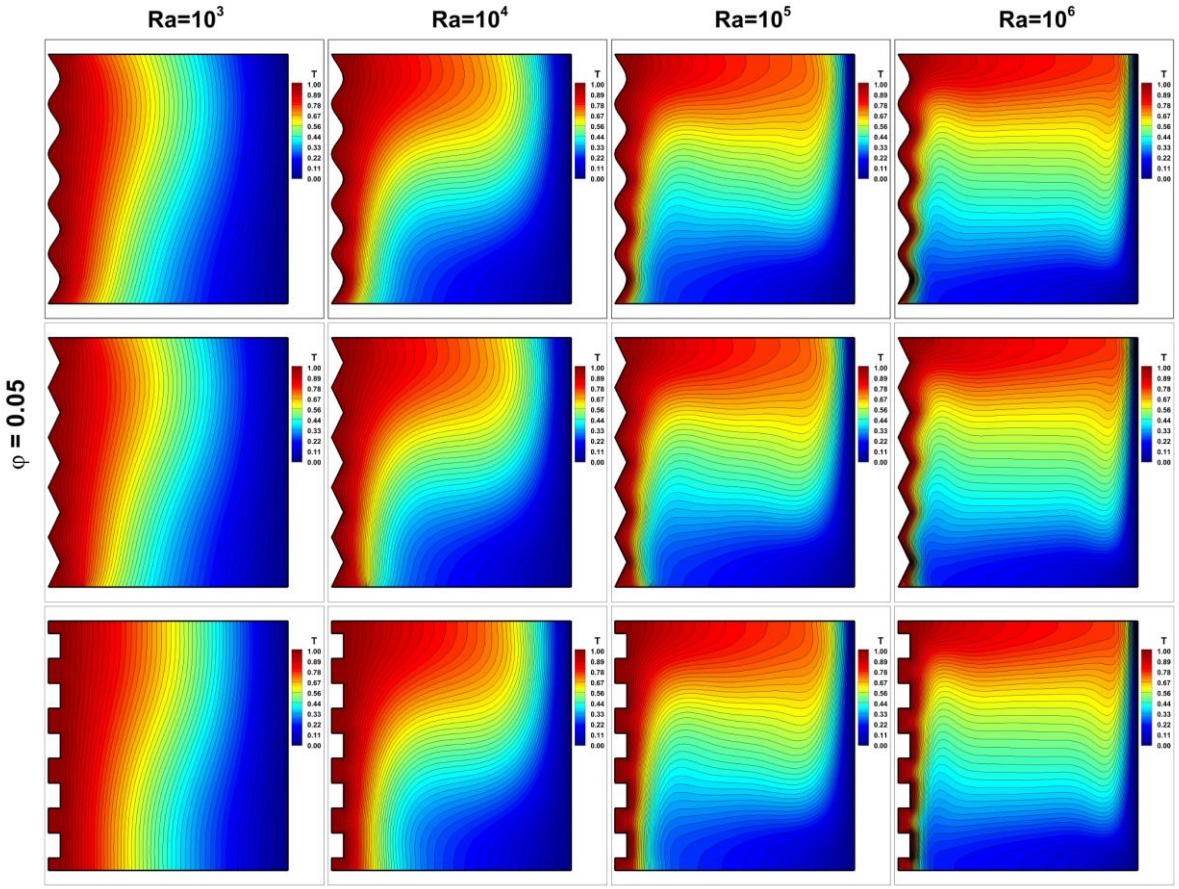

Fig 2. Distribution of isotherms inside the square cavity with one irregular wall of different shapes for different numbers of Ra, and the values of ϕ= 0.05

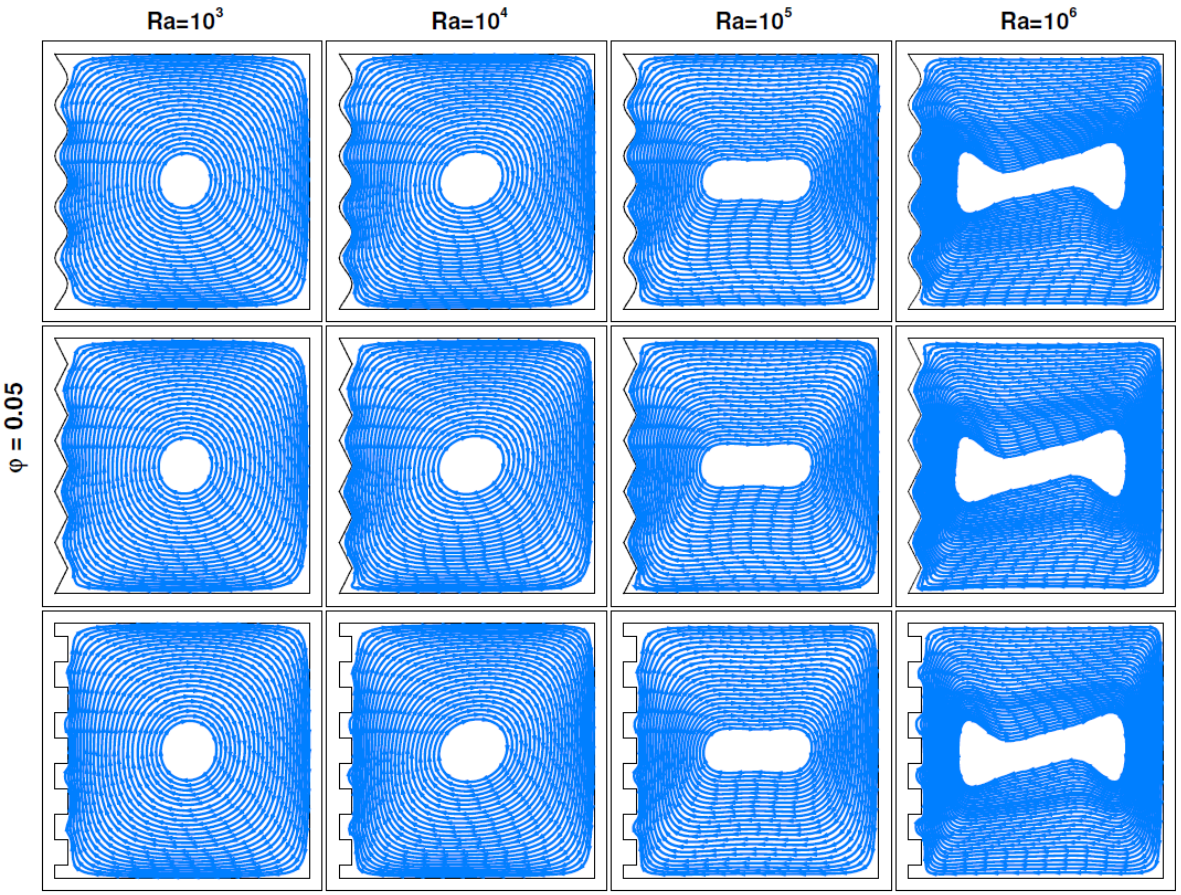

Fig 3. Distribution of streamlines inside the square cavity with one irregular wall of different shapes for different numbers of Ra, and the values of Φ = 0.05

the wall's curvature. We can see that, for low Rayleigh numbers and across all configurations, the isotherms are parallel to the vertical walls, indicating that conduction is dominant. As the Rayleigh number increases, the shape of the isotherms transforms and becomes parallel to the horizontal walls, signifying that convection is dominant. Additionally, the density of the isotherms near the cold and hot walls increases as the Rayleigh number increases, indicating an increase in the temperature gradient and, therefore, an increase in the rate of heat transfer along these walls. With an increase in the volume fraction of nanoparticles, the isotherms changed slightly. This is due to the increased viscosity of the fluid flow caused by the nanoparticles, which slows down the flow and decreases the natural convection mechanism, potentially reducing the rate of heat transfer. However, the overall rate of heat transfer throughout the cavity improved due to the increased thermal conductivity of the base fluid.

In Figure 3, the streamlines are depicted for different values of the Rayleigh number and volume fractions of nanoparticles. As seen in the figure, the flow is characterized by a single vortex in the center of the cavity for all parameters and configurations. This vortex arises from the movement of fluid within the cavity, which is driven by the difference in density between the cold and hot walls. At low Rayleigh numbers, the fluid moves at a slow velocity, leading to conduction being dominant. As the Rayleigh number increases, the buoyancy force increases, causing the fluid to move faster within the cavity and leading to an increase in velocity and temperature gradients, making convection dominant. It is also noted that the size of the central vortex increases as the Rayleigh number increases, and this effect is more pronounced at higher values. Additionally, the density of the streamlines near the vertical walls increases, indicating an increase in the temperature gradient and improved heat transfer rate. The density of the streamlines also increases with an increase in the volume fraction of nanoparticles, due to the high energy transported by the flow caused by the irregular motion of the nanoparticles. The flow characteristics remain the same in each case, except for the region with the highest temperature, where the streamlines take on the shape of the heated wall. It's important to note that the thermal lines and streamlines do not provide enough information about the influence of the irregular wall, so it is recommended to analyze the Nusselt number.

The local Nusselt numbers for different values of the Rayleigh number at a volume fraction of $\phi = 0.05$ for corrugated walls are depicted in Figure 4. The results show that the local Nusselt number exhibits a consistent behavior in each case. Additionally, it is observed that the Nusselt number increases at each crest due to the irregularity in the shape that causes more fluid particles to come into contact with the heated wall. An increase in the Rayleigh number results in an enhancement of the buoyancy force and the fluid velocity in the cavity, which in turn leads to an increase in the local Nusselt number.

The variation of the average Nusselt number with respect to the Rayleigh number is also shown in Figure Figure 4 for regular and corrugated walls. The results indicate that when the regular wall is replaced with an irregular wall, the average Nusselt number increases more for the wavy wall compared to the regular wall and decreases for both the zigzag and square walls. This is because the fluid particles flow smoothly on wavy wall more than zig-zag or square, where they get stuck in confined areas. In addition, the wavy shape increases the

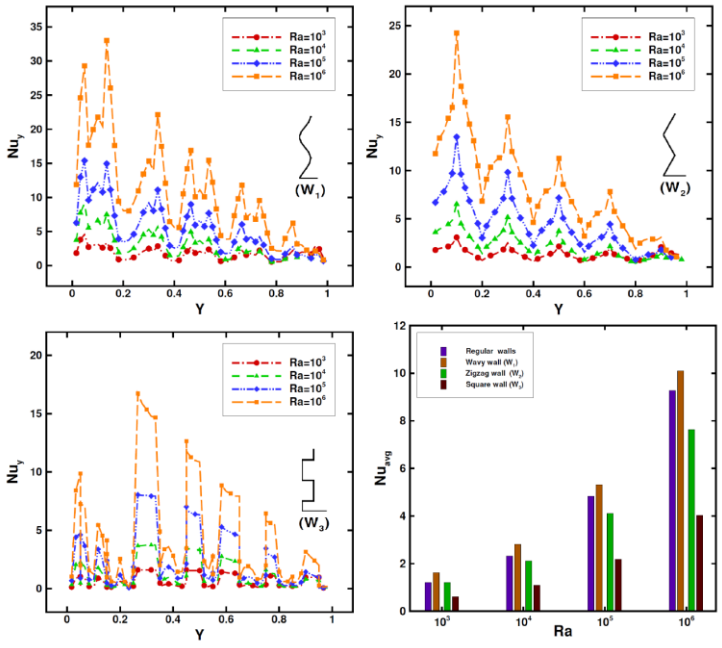

Fig 4. Local and average Nusselt numbers on the hot irregular left lateral wall with different shapes for various Rayleigh numbers at ϕ= 0.05

Table 4
The variation of the average Nusselt number on the hot regular and irregular walls for different volume fractions of nanoparticles at the value of Ra =10^5

Volume fraction of nanoparticles	Type of wall	Average Nusselt number
$\phi = 0.05$	Regular	4.63
	Wavy	6.1314
	Zigzag	3.8013
	Square	2.3849
$\phi = 0.1$	Regular	5.0012
	Wavy	6.4042
	Zigzag	3.9479
	Square	2.4717

surface area of heat transfer compared to other configurations, resulting in a higher average Nusselt number.

Finally, the variation of the average Nusselt number on the hot wall for different volume fractions of nanoparticles at $Ra = 10^5$ for regular and irregular walls is analyzed and presented in Table 4. For all cases, it can be seen that the average Nusselt number increases with an increase in the volume fraction of nanoparticles, which is due to the improvement in the thermal conductivity of the base fluid caused by the addition of nanoparticles. The wavy wall keeps their higher efficiency compared to other corrugated or flat walls.

4.3 Natural convection in a square cavity with two irregular lateral walls

In this section of the study, the right and left vertical walls were considered corrugated, while the remaining walls were considered flat surfaces. The results demonstrate the impact of the two corrugated vertical walls, Rayleigh number, and nanoparticle volume fraction on the heat transfer rate.

The distribution of isothermal lines inside three cavities for various Rayleigh numbers and two volume fractions of nanoparticles ϕ = 0.05 and 0.1, is shown in Figure 5. Except for the areas with hot and cold walls, where the isotherms distort into the shape of corrugated walls, the behavior of the isotherms is identical across all configurations. When the Rayleigh number is low, the isotherms are more vertical, which indicates that heat transfer is dominated by conduction. As the Rayleigh number increases, the isotherms begin to deform and become more pronounced, especially in the center of the cavities, which suggests that heat transfer through convection is becoming more dominant. The density of isothermal lines near the corrugated hot and cold walls is also increased, which strengthens the temperature gradient and leads to an increased rate of heat transfer. With increasing volume fraction of nanoparticles, the conductivity of the base fluid increases, and the density of isotherms becomes more significant near the vertical walls, causing the deformation of the isotherms to also

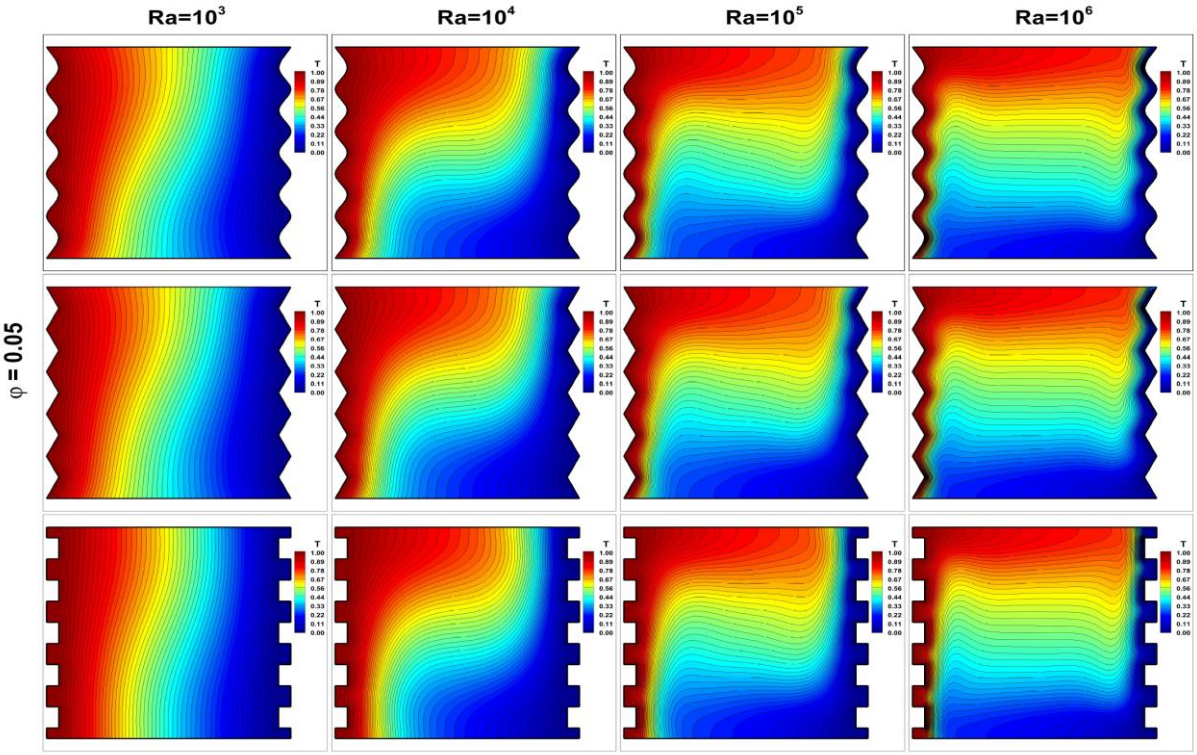

Fig 5. Distribution of isotherms inside the square cavity with two irregular walls of different shapes for different numbers of Ra, and the values of ϕ= 0.05.

increase. As a result, the heat transfer rate from the walls increases.

Figure 6 shows the distribution of streamlines inside the cavity with different shapes of vertical hot and cold walls for various Rayleigh numbers and volume fractions of nanoparticles. At a fixed Rayleigh number, the flow pattern is qualitatively the same across all configurations, especially in the middle of the cavity where a clockwise recirculation vortex is formed. The streamlines on the left and right sides of the cavity are compressed due to the irregularity of the corrugated walls, while those on the top and bottom are not affected. As the Rayleigh number increases, the clockwise symmetric recirculation vortex observed at Ra = 10^3 disappears and is replaced by two small recirculation vortexes near the corrugated walls for Ra = 10^6. The density of the streamlines is enhanced near the hot and cold walls with increasing Rayleigh

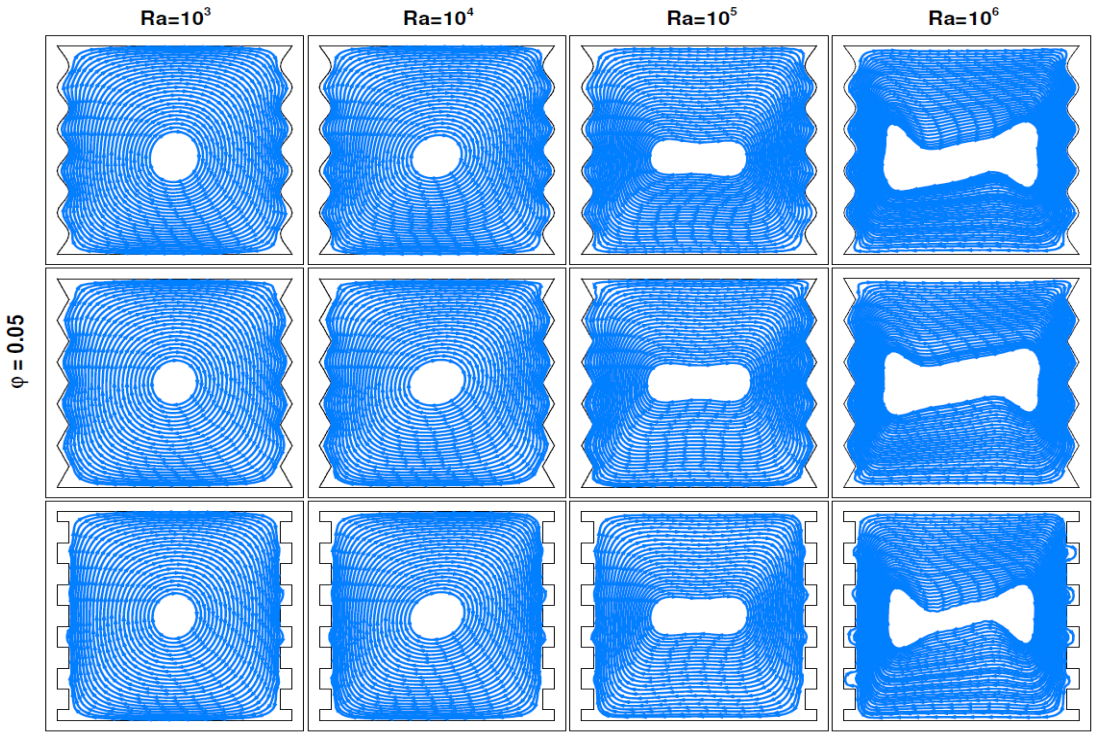

Fig 6. Distribution of streamlines inside the square cavity with two irregular walls of different shapes for different numbers of Ra, and the values of ϕ= 0.05.

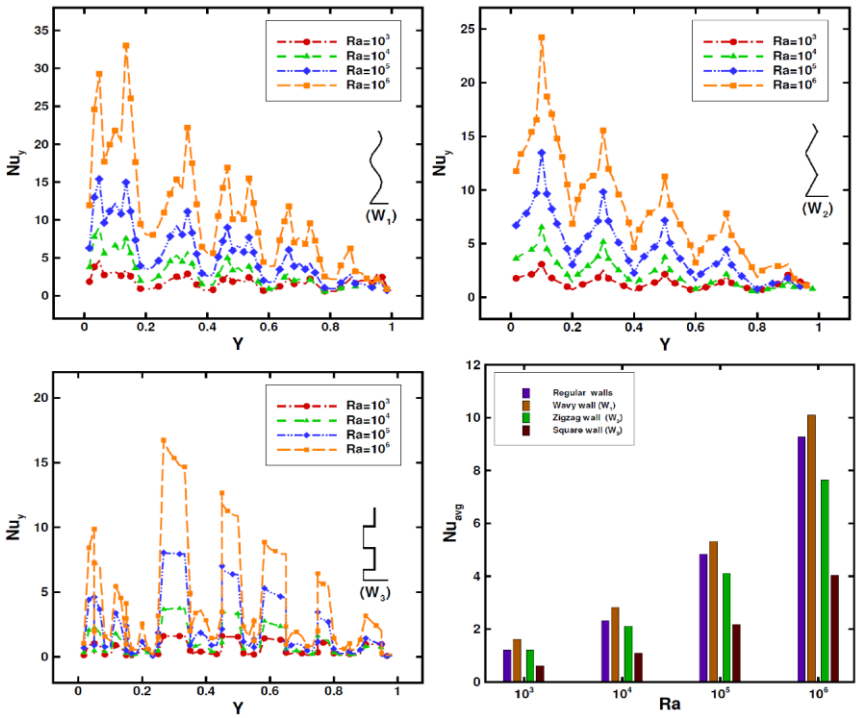

Fig 7. Local and averaged Nusselt number along the irregular walls for various Rayleigh numbers at ϕ= 0.05

Table 5
The variation of the average Nusselt number along the regular and irregular walls for different volume fractions of nanoparticles at the value of Ra =10^5

Volume fraction of nanoparticles	Type of wall	Average Nusselt number
ϕ=0.05	Regular	4.83
	Wavy	5.1348
	Zigzag	4.1079
	Square	2.1784
ϕ=0.1	Regular	5.0012
	Wavy	5.5545
	Zigzag	2.2859
	Square	2.262

number, indicating an increase in the temperature gradient and a higher rate of heat transfer. Additionally, the velocity of the recirculation vortex also increases, contributing to improved heat transfer inside the cavity. With an increase in the volume fraction of nanoparticles, the density of the streamlines also rises, further improving heat transfer.

The illustration of the variation of the local Nusselt number for different values of the Rayleigh number at ϕ = 0.05 is shown in the Figure 7 for all corrugated walls. It can be observed that the Nusselt number increases at the high peaks and decreases at the lower peaks of the hot corrugated wall, which is due to the irregular shape of the walls. The irregular shape allows more fluid particles to come into contact with the higher peaks, resulting in an increase in the local Nusselt number at those locations compared to the lower peaks where the number of fluid particles in contact with the wall decreases, leading to a decrease in the local Nusselt number. This is evident in Figure 6, particularly on the cavity with square corrugated vertical walls. It is also noted that the local Nusselt number for wavy walls is larger than for other configurations. For the triangular zigzag and square walls, fluid particles move up and down due to their corrugated shapes, causing a backflow that decreases the fluid flow rate. However, this phenomenon does not occur in the case of wavy hot walls, making the heat transfer rate higher in the wavy wall compared to the triangular and zig-zag walls. Additionally, the local Nusselt number increases with the increasing Rayleigh number, as the increase in the Rayleigh number enhances convection and improves heat transfer due to the increase in buoyancy forces inside the cavity.

The variation of the average Nusselt number versus the Rayleigh number for regular and corrugated walls at ϕ = 0.05 is also shown in same figure. The figure reveals a reduction in the average value of the Nusselt number for cavities with zig-zag and square walls compared to the regular cavity and wavy cavity. Also, the Nusselt number for the wavy wall increased more than regular cavity or cavities with zig-zag and square walls, with the increase observed for all values of the Rayleigh

number and larger for high values. At low Rayleigh numbers, the triangular square wall has no significant impact on the average Nusselt number compared to the other configurations, where the Nusselt number was increasing for the wavy wall and decreasing for the square wall for the same reasons mentioned before with one irregular wall.

To summarize, the Table 5 shows the variation of the average Nusselt number on the hot wall of the cavity for two volume fractions of nanoparticles for the regular and all corrugated walls, with the Rayleigh number kept constant at 10^5. The Table reveals that for all configurations considered, the average Nusselt number increases with an increase in the volume fraction of nanoparticles. This is because an increase in the volume fraction of nanoparticles leads to an increase in the thermal conductivity of the base fluid, which in turn increases the heat transfer rate.

5. Conclusions

The study investigates the effect of different wall, and the impact of the Rayleigh number and volume fraction of nanoparticles on natural convection in a square cavity filled with a mixture of Al_2O_3 solid particles and liquid water. The results of numerical simulations showed that the overall temperature distribution remained unchanged except near the hot wall, and the flow was dominated by convection as the Rayleigh number increased. The heat transfer rate improved with an increase in the volume fraction of nanoparticles. The flow was characterized by a central vortex that increased in size as the Rayleigh number increased. The average Nusselt number was found to be highest with the wavy wall, and to increase with an increase in the volume fraction of nanoparticles.

Author Contributions: Y.E.: Conceptualization, methodology, formal analysis, writing—original draft, M.J.; resources, project administration, C.E.; Conceptualization, methodology, writing—review and editing, project administration, validation, B.D.; writing—review. All authors have read and agreed to the published version of the manuscript.

Funding: The authors received no financial support for the research, authorship, and/or publication of this article.

Conflicts of Interest: The authors declare no conflict of interest.

References

Aghakhani, S., Pordanjani, A. H., Karimipour, A., Abdollahi, A., &Afrand, M. (2018). Numerical investigation of heat transfer in a power-law non-newtonian fluid in a C-shaped cavity with magnetic field effect using finite difference lattice Boltzmann method. *Computers & Fluids*, *176*, 51–67. https://doi.org/10.1016/j.compfluid.2018.09.012

Al Nuwairan M., Chaabelasri E. (2023), Numerical Assessment of Nanofluid Natural Convection Using Local RBF Method Coupled with an Artificial Compressibility Model. *Computer Modeling in Engineering & Sciences*, 135, 1526-1506. https://doi.org/10.32604/cmes.2022.022649

Alqaed S., Mustafa J., Sharifpur M., (2022) Numerical investigation and optimization of natural convection and entropy generation of alumina/H2O nanofluid in a rectangular cavity in the presence of a magnetic field with artificial neural networks, *Engineering Analysis with Boundary Elements*, 140, 507-518, https://doi.org/10.1016/j.enganabound.2022.04.034

Aminossadati, S. M., &Ghasemi, B. (2009). Natural convection cooling of a localised heat source at the bottom of a nanofluid-filled enclosure. *European Journal of Mechanics. B, Fluids*, 28(5), 630–640. https://doi.org/10.1016/j.euromechflu.2009.05.006

Bairi, A., Zarco-Pernia, E. & Garcia de Maria, J.M. (2014), A review on natural convection in enclosures for engineering applications. The particular case of parallelogrammic diode cavity. *Applied Thermal Engineering*, 63, pp. 304–322. https://doi.org/10.1016/j.applthermaleng.2013.10.065

Basak, T., Chamkha, A. J. (2012). Heatline analysis on natural convection for nanofluids confined within square cavities with various thermal boundary conditions. *International Journal of Heat and Mass Transfer*, 55(21–22),5526–5543. https://doi.org/10.1016/j.ijheatmasstransfer.2012.05.025.

Bayona, V., Moscoso, M., &Kindelan, M. (2011). Optimal constant shape parameter for multiquadric based RBF-FD method. *Journal of Computational Physics*, 230(19), 7384–7399. https://doi.org/10.1016/j.jcp.2011.06.005

Bejan, A. (2013). Convection heat transfer. John wiley& sons. https://onlinelibrary.wiley.com/doi/book/10.1002/9781118671627

Brinkman, H. C. (1952). The viscosity of concentrated suspensions and solution. *The Journal of Chemical Physics*, 20, 571–581. https://doi.org/10.1063/1.1700493.

Chaabelasri E., Jeyar M., Borthiwick A.G.L. (2019), Explicit radial basis function collocation method for computing shallow water flows *Procedia Computer Science*. 148, 361-370. https://doi.org/10.1016/j.procs.2019.01.044

Chorin, A. (1997). A numerical method for solving incompressible viscous flow problems. *Journal of Computational Physics*, 135(2), 118–125. https://doi.org/10.1006/jcph.1997.5716.

Das, D., Roy, M. &Basak, T. (2017), Studies on natural convection within enclosure of various (non-square) shapes: A review. International *Journal of Heat and Mass Transfer*, 106, pp. 356–406.

Fasshauer, G. E., & Zhang, J. G. (2007). On choosing "optimal" shape parameters for RBF approximation. *Numerical Algorithms*, 45(1–4), 345–368. https://doi.org/10.1007/s11075-007-9072-8

Hu YP., Wang FJ, Zhang YC., Li YR., Li MH. (2022), Oscillatory natural convection of Al2O3-water nanofluid near its density maximum in a narrow horizontal annulus, *International Communications in Heat and Mass Transfer*. 136, 106207, https://doi.org/10.1016/j.icheatmasstransfer.2022.106207

Jeyar, M., Chaabelsri, E., Bensaad, M., &Achemlal, D. (2022). A meshless numerical method based on rbf with artificial compressibility to simulate natural heat convection in enclosed cavities. *JP Journal of Heat and Mass Transfer*, 28, 15–34. https://doi.org/10.17654/0973576322031

Kadhim, H. T., Al-Manea, A., Al-Shamani, A. N., &Yusaf, T. (2022). Numerical analysis of hybrid nanofluid natural convection in a wavy walled porous enclosure: Local thermal non-equilibrium model. *International Journal of Thermofluids*, 15(100190), 100190. https://doi.org/10.1016/j.ijft.2022.100190

Kansa, E. J. (1990). Multiquadrics-A scattered data approximation scheme with applications to computational fluid-dynamics-I surface approximations and partial derivative estimates. *Computers & Mathematics with Applications*, 19(8–9), 127–145. https://doi.org/10.1016/0898-1221(90)90270-T.

Keshtkar, M. M., &Talebizadehsardari, P. (2018). Investigation of transient conduction–radiation heat transfer in a square cavity using combination of LBM and FVM. *Sadhana*, 43(4). https://doi.org/10.1007/s12046-018-0854-6

Khanafer, K., Vafai, K., & Lightstone, M. (2003). Buoyancy-driven heat transfer enhancement in a two-dimensional enclosure utilizing nanofluids. *International Journal of Heat and Mass Transfer*, 46(19), 3639–3653. https://doi.org/10.1016/s0017-9310(03)00156-x

Liu, C.-S., & Liu, D. (2018). Optimal shape parameter in the MQ-RBF by minimizing an energy gap functional. *Applied Mathematics Letters*, 86, 157–165. https://doi.org/10.1016/j.aml.2018.06.031

Luo, K., Ai, Q., Yi, H.-L., & Tan, H.-P. (2015). Coupled lattice Boltzmann and meshless simulation of natural convection in the presence of volumetric radiation. *Journal of Heat Transfer*, 137(11), 111504. https://doi.org/10.1115/1.4030904

Mahmoodi, M., &Sebdani, S. M. (2012). Natural convection in a square cavity containing a nanofluid and an adiabatic square block at the center. *Superlattices and Microstructures*, 52(2), 261–275. https://doi.org/10.1016/j.spmi.2012.05.007

Maxwell, J. (1904). A treatise on electricity and magnetism, 2nd edition. Cambridge, UK: *Oxford,University Press*.

Miroshnichenko, I. V., &Sheremet, M. A. (2018). Turbulent natural convection heat transfer in rectangular enclosures using experimental and numerical approaches: A Review. *Renewable and Sustainable Energy Reviews*, *82*, 40–59. https://doi.org/10.1016/j.rser.2017.09.005

Muhammad, N., Nadeem, S., &Issakhov, A. (2020). Finite volume method for mixed convection flow of ag–ethylene glycol nanofluid flow in a cavity having thin central heater. *Physica A: Statistical Mechanics and Its Applications*, *537*, 122738. https://doi.org/10.1016/j.physa.2019.122738

Najafi, M., &Enjilela, V. (2014). Natural convection heat transfer at high Rayleigh numbers – Extended meshless local Petrov–Galerkin (MLPG) primitive variable method. *Engineering Analysis with Boundary Elements*, 44, 170–184. https://doi.org/10.1016/j.enganabound.2014.01.022

PekmenGeridonmez B., Oztop H.F. (2022), The effect of inclined periodic magnetic field on natural convection flow of Al2O3-Cu/water nanofluid inside right isosceles triangular closed spaces, *Engineering Analysis with Boundary Elements*, 141, 222-234. https://doi.org/10.1016/j.enganabound.2022.05.009

Pranowo, &Wijayanta, A. T. (2021). Numerical solution strategy for natural convection problems in a triangular cavity using a direct meshless local Petrov-Galerkin method combined with an implicit artificial-compressibility model. *Engineering Analysis with Boundary Elements,* 126, 13–29. https://doi.org/10.1016/j.enganabound.2021.02.006

Rahimi, A. Sae, A.D., Kasaeipoor, A.D. &Malekshah, E.A. (2019), A comprehensive review on natural convection flow and heat transfer. *International Journal of Numerical Methods for Heat and Fluid Flow*, 29(3), 834–887. https://doi.org/10.1108/HFF-06-2018-0272

Saleh, H., Roslan, R., & Hashim, I. (2011). Natural convection heat transfer in a nanofluid-filled trapezoidal enclosure. *International Journal of Heat and Mass Transfer*, 54(1–3), 194–201. https://doi.org/10.1016/j.ijheatmasstransfer.2010.09.053

Sarra, S. A. (2012). A local radial basis function method for advection-diffusion-reaction equations on complexly shaped domains. *Applied Mathematics and Computation*, 218(19), 9853–9865. https://doi.org/10.1016/j.amc.2012.03.062.

Shahsavar Ma, Y., Moradi A., Rostami I., Moradikazerouni S., Yarmand S. , Zulkifli, N. W. (2021). Using finite volume method for simulating the natural convective heat transfer of nano-fluid flow inside an inclined enclosure with conductive walls in the presence of a constant temperature heat source. *Physica A: Statistical Mechanics and Its Applications*, *580*, 123035. https://doi.org/10.1016/j.physa.2019.123035

Sheikhi, N., Najafi, M., &Enjilela, V. (2018). Solving natural convection heat transfer in turbulent flow by extending the meshless local Petrov–Galerkin method. *Engineering Analysis with Boundary Elements*, 93, 29–43. https://doi.org/10.1016/j.enganabound.2018.03.018

Sheikholeslami, M., &Ganji, D. D. (2016). Nanofluid convective heat transfer using semi analytical and numerical approaches: A review. *Journal of the Taiwan Institute of Chemical Engineers*, 65, 43–77. https://doi.org/10.1016/j.jtice.2016.05.014

Sheikhzadeh, G. A., Arefmanesh, A., Kheirkhah, M. H., &Abdollahi, R. (2011). Natural convection of Cu–water nanofluid in a cavity with partially active side walls. *European Journal of Mechanics. B, Fluids*, 30(2), 166–176. https://doi.org/10.1016/j.euromechflu.2010.10.003

Shoeibi, S., Kargarsharifabad, H., Sharifpur, M., & Meyer, J. P. (2023). Hybrid nanofluid natural convection in the square enclosure with periodic magnetic field: experimental investigation and economic evaluation. *Journal of Thermal Analysis and Calorimetry*. https://doi.org/10.1007/s10973-022-11924-1

Sophy, T., Sadat, H., &Prax, C. (2002). A meshless formulation for three-dimensional laminar natural convection. *Numerical Heat Transfer Part B Fundamentals*, 41(5), 433–445. https://doi.org/10.1080/104077902753725894

Uddin, M. (2014). On the selection of a good value of shape parameter in solving time-dependent partial differential equations using RBF approximation method. *Applied Mathematical Modelling*, 38(1), 135–144. https://doi.org/10.1016/j.apm.2013.05.060

Zarei M.S., Khalil Abad A.T., Hekmatifar M., Toghraie D. (2022), Heat transfer in a square cavity filled by nanofluid with sinusoidal wavy walls at different wavelengths and amplitudes, *Case Studies in Thermal Engineering*, 34, 101970. https://doi.org/10.1016/j.csite.2022.101970

Zhang, X., & Zhang, P. (2015). Meshless modeling of natural convection problems in non-rectangular cavity using the variational multiscale element free Galerkin method. *Engineering Analysis with Boundary Elements*, 61, 287–300. https://doi.org/10.1016/j.enganabound.2015.08.005